Targeted molecular dynamics simulation studies of calcium binding and conformational change in the C-terminal half of gelsolin

ARTICLE *in* BIOCHEMICAL AND BIOPHYSICAL RESEARCH COMMUNICATIONS · MAY 2006

Impact Factor: 2.3 · DOI: 10.1016/j.bbrc.2006.01.184 · Source: PubMed

6 AUTHORS, INCLUDING:

Robert C Robinson
Agency for Science, Technology and Resear…
101 PUBLICATIONS **2,684** CITATIONS
SEE PROFILE

Han Choe
Asan Medical Center
83 PUBLICATIONS **1,290** CITATIONS
SEE PROFILE

Available online at www.sciencedirect.com
SCIENCE DIRECT
Biochemical and Biophysical Research Communications 342 (2006) 702–709
BBRC
www.elsevier.com/locate/ybbrc

Targeted molecular dynamics simulation studies of calcium binding and conformational change in the C-terminal half of gelsolin

Hui Sun Lee [a,c], Robert Charles Robinson [d], Chul Hyun Joo [a,c], Heuiran Lee [a,c], Yoo Kyum Kim [a,c,*], Han Choe [b,c,*]

[a] Department of Microbiology, University of Ulsan College of Medicine, 388-1 PoongNap-dong Songpa-goo, Seoul 138-736, South Korea
[b] Department of Physiology, University of Ulsan College of Medicine, 388-1 PoongNap-dong Songpa-goo, Seoul 138-736, South Korea
[c] Research Institute for Biomacromolecules, University of Ulsan College of Medicine, 388-1 PoongNap-dong Songpa-goo, Seoul 138-736, South Korea
[d] Institute of Molecular and Cell Biology, Proteos, 61 Biopolis Drive, 138673 Singapore, Singapore

Received 30 December 2005
Available online 13 February 2006

Abstract

Gelsolin consists of six related domains (G1–G6) and the C-terminal half (G4–G6) acts as a calcium sensor during the activation of the whole molecule, a process that involves large domain movements. In this study, we used targeted molecular dynamics simulations to elucidate the conformational transitions of G4–G6 at an atomic level. Domains G4 and G6 are initially ruptured, followed by a rotation of G6 by ~90°, which is the dominant conformational change. During this period, local conformational changes occur at the G4 and G5 calcium-binding sites, facilitating large changes in interdomain distances. Alterations in the binding affinities of the calcium ions in these three domains appear to be related to local conformational changes at their binding sites. Analysis of the relative stabilities of the G4–G6-bound calcium ions suggests that they bind first to G6, then to G4, and finally to G5.

Keywords: Gelsolin C-terminal half; Calcium binding; Conformational change; Targeted molecular dynamics simulation

Regulation of actin dynamics requires the spatial and temporal control of the assembly and disassembly of actin filaments. These mechanisms allow actin polymerization to drive processes such as cell shape change, motility, and platelet activation. Gelsolin is an actin filament severing, capping, and uncapping protein that is involved in the regulation of actin filament length [1–3]. In the presence of Ca^{2+}, gelsolin severs pre-existing actin filaments and caps their barbed ends. The barbed-end cap is highly stable even in the absence of Ca^{2+}. Gelsolin-capped filaments are uncapped by phosphoinositides, particularly a phosphatidylinositol 4,5-bisphosphate (PIP_2), to allow polymerization to be initiated [4,5]. Actin-depolymerizing factor (ADF)/cofilin synergizes with gelsolin through preferential binding to gelsolin-capped filaments, resulting in the rapid depolymerization of gelsolin-capped actin filaments [6].

Gelsolin comprises six structurally similar domains, designated G1–G6 [7], which appear to have evolved through a gene triplication process followed by an additional duplication [8]. The structure of G1 is organized around a central five-stranded mixed β-sheet that is sandwiched between a long α-helix running approximately parallel to the strands and a shorter α-helix running approximately perpendicular to the strands [9]. The structural similarity is strongest for the domains between the two halves of gelsolin, namely between G1 and G4, G2 and G5, and G3 and G6 [7]. Hence, gelsolin can be divided into two domain triplets of the N- and C-terminal halves, G1–G3 and G4–G6, respectively.

The structure of full-length gelsolin determined in a Ca^{2+}-free environment revealed that the domains form a compact entity [7]. In this inactive structure, gelsolin

* Corresponding authors. Fax: +82 2 3010 8119.
E-mail addresses: ykkim@amc.seoul.kr (Y.K. Kim), hchoe@amc.seoul.kr (H. Choe).

0006-291X/$ - see front matter © 2006 Elsevier Inc. All rights reserved.
doi:10.1016/j.bbrc.2006.01.184

cannot bind to actin because the actin-binding surfaces are sterically masked (Fig. 1A). The domains of gelsolin are secured in this state by latching of the G6 C-terminal extension onto G2 and by the joining of the first and third domains of each half of gelsolin through extended interdomain β-sheets. Activation of gelsolin at physiological pH is induced by calcium ions (Fig. 1B). Upon Ca^{2+} binding, gelsolin releases the G6 tail latch from G2 and severs the extended interdomain β-sheets in each half of the molecule. These conformational changes expose the major actin-binding sites on G1, G2–G3, and G4 [7,10,11].

A variety of evidence indicates that G4–G6 acts as the overall calcium sensor in whole gelsolin. Isolated G4–G6 has an absolute requirement for Ca^{2+} to bind to actin, whereas isolated G1–G3 is active in the absence of Ca^{2+}, although its efficiency is enhanced by Ca^{2+} [12,13]. These observations suggest that the Ca^{2+}-dependent structural changes in G4–G6 are a major factor controlling the actin-binding properties of the whole protein. Analysis of the structures of Ca^{2+}-activated gelsolin both in the presence and absence of actin clearly shows that the major conformational changes are induced by Ca^{2+} binding and not through interaction with actin [14–16].

Several studies have reported the biophysical and biochemical characteristics of the Ca^{2+} activation of gelsolin. However, the assignment of the relative binding affinities to individual Ca^{2+}-binding sites and the detailed mechanism of the sequence of conformational changes induced by Ca^{2+}-binding remains in question. In the present study, we used molecular dynamics (MD) simulations to explore the conformational changes in G4–G6 induced by Ca^{2+} in silico. In particular, we performed MD simulations with external perturbations, which are termed targeted molecular dynamics (TMD) simulations, to observe possible pathways of conformational change between the inactive and active structures.

Materials and methods

The inactive form of G4–G6 in Ca^{2+}-free conditions was obtained from the 2.5 Å X-ray crystal structure of full-length horse plasma gelsolin (PDB entry 1D0N) (Fig. 1A) [7]. The structure spanning from Asp414 to Trp741 of chain A was used. The structure of the active form of G4–G6 was constructed based on the 2.0 Å X-ray crystal structure of human gelsolin (PDB entry 1P8X) (Fig. 1B) [16]. This structure contains three Ca^{2+} ions, in G4, G5, and G6, which were denoted IIG4, IIG5, and IIG6, respectively. Only the structure spanning from Asp414 to Trp741 of chain B was used. In this study, we define the domains G4, G5, and G6 as spanning residues 414–513, 514–619, and 620–741, respectively. There are three missing residues in the activated structure (Gly456-Arg458); these were modeled by ModLoop [17]. The N- and C-termini were capped with a neutral acetyl and an N-methyl group, respectively.

The CHARMM 19 polar hydrogen force field with the implicit solvation function EEF1 [18] was used in this study. The nonbonding parameters for a Ca^{2+} ion were obtained from the CHARMM 27 parameter file because the CHARMM 19 parameter file does not contain any nonbonding parameters for Ca^{2+} ions. For EEF1 implicit solvation model calculations, the parameters were set as follows: (1) the atomic volume of a Ca^{2+} ion was calculated using half of the Lennard-Jones collision diameter; (2) the free energy of solvation of a Ca^{2+} ion was set to −359.7 kcal/mol [19]; (3) the correlation length was optimized through a series of 50 ps MD simulations, and the optimum correlation length was chosen to be that with the smallest distance deviations from the original coordinates in the crystal structure (data not shown).

The pathways between inactivated and activated conformations were explored using TMD simulations [20]. TMD simulation is a method for observing reaction paths between two conformations of a molecule by continuously decreasing the distance to the target conformation. This is accomplished by adding a harmonic potential energy term of the form

$$W_{\mathrm{TMD}} = k_{\mathrm{TMD}}(\mathrm{RMSD} - \rho)^2, \quad (1)$$

where W_{TMD} is the biasing potential energy in kcal/mol during the TMD simulation, k_{TMD} is a force constant, RMSD is the root-mean-square deviation from the target structure, and ρ is the desired RMSD value. The initial value of ρ is set as the RMSD between the initial and target structures. During the simulation, ρ is gradually decreased to zero. If the RMSD spontaneously decreases in the simulation step from t to $t + \Delta t$ (i.e., $\mathrm{RMSD} < \rho$), the external perturbation is zero and has no effect on the

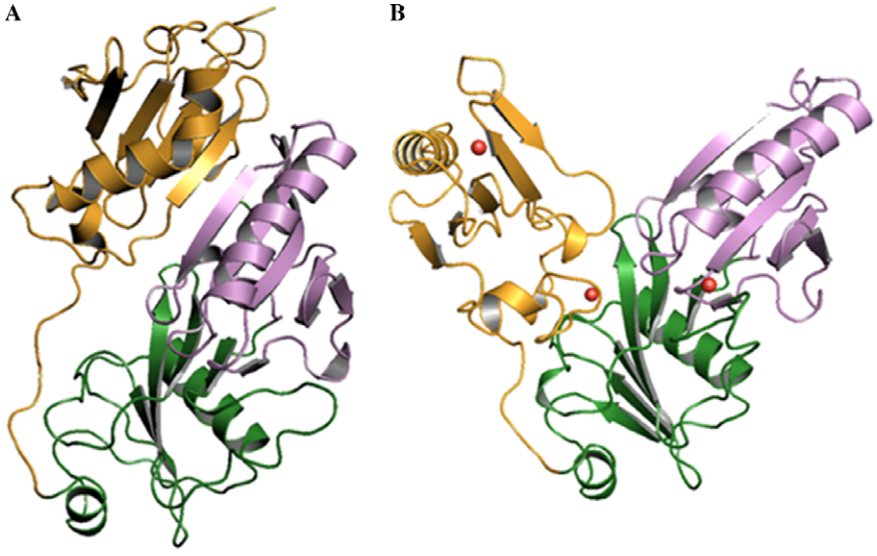

Fig. 1. Ribbon representation of the C-terminal half of gelsolin (denoted as G4–G6 in this study). G4 is shown in pink, G5 in green, and G6 in orange. (A) G4–G6 from the inactive gelsolin structure (PDB entry 1D0N). (B) G4–G6 in the presence of calcium ions (PDB entry 1P8X). Ca^{2+} ions are shown as red spheres. (For interpretation of the references to color in this figure legend, the reader is referred to the web version of this paper.)

dynamics. In the activation-to-inactivation TMD simulation, active G4–G6 and inactive G4–G6 were used as the initial and target structures, respectively.

All simulations and data analyses were performed using SELF-ASSEMBLER, an MD simulation program that we developed, with an integration step of 2 fs. The structures of active and inactive gelsolin G4–G6 were subjected to energy minimization to relieve possible steric clashes and overlapping of side-chains. The bond lengths involving hydrogen atoms were fixed using a SHAKE algorithm [21]. Initial velocities of atoms were assigned from the Boltzmann distribution and then gradually heated to 300 K at a speed of 5 °C/200 steps. The temperature of the system was maintained using a Nose–Hoover thermostat [22]. All initial structures for the TMD simulations were equilibrated at 300 K for 500 ps. For Ca^{2+}-containing active G4–G6, the structure was equilibrated with Ca^{2+} ions that were harmonically constrained in their binding sites. We observed that the total energies of the structures were stably maintained during the equilibrium MD simulations (data not shown). To measure the rotational angles of G6, we chose four points, A, B, C, and D, such that point A is the CA atom of the first residue (Gly514) in the G5 domain, point B corresponds to the center of mass (CM) of the G5 domain, point C is the CM of the G6 domain from which residues within G6 long helix are excluded, and point D is the CM of the G6 long helix containing residues Glu690 to Ala709. The rotational angle of G6 was defined as the dihedral angle between planes ABC and BCD.

Results

Conformational change in G4–G6 during activation-to-inactivation TMD simulation

To investigate the transition mechanism of gelsolin G4–G6, we carried out activation-to-inactivation TMD simulations. The trajectories obtained from the TMD simulations allow us to suggest a likely pathway of conformational change during G4–G6 activation. We performed these simulations with various constraint force constants to determine the most reasonable pathway for conformational change. However, we could not observe a reasonable pathway for the conformation changes within 2 ns. The small constraint force constants were too weak to simulate the full pathway. On the other hand, large constraint force constants caused distortions of the secondary structures in G4 and G6. Therefore, we carried out the activation-to-inactivation TMD simulation in two stages. In the first stage, ρ was set as the RMSD between the initial and target structures and gradually decreased to zero for a 2 ns TMD simulation. In the second stage, an additional 2 ns simulation was performed with ρ set to zero.

TMD simulations are performed with restraints to transform a sample conformation into a target conformation with a desired RMSD. The bias energy, which is the magnitude of external perturbation, plays a role in expediting the conformational changes during which the conformation is trapped in a local minimum. Therefore, the bias energy accelerates the conformational changes along the pathway from the initial conformation to the target conformation. When the conformational changes occur, the RMSD between the sample and the target is reduced. Fig. 2A shows a profile of RMSD as a function of simulation time. Initially, the RMSD in the active G4–G6 from

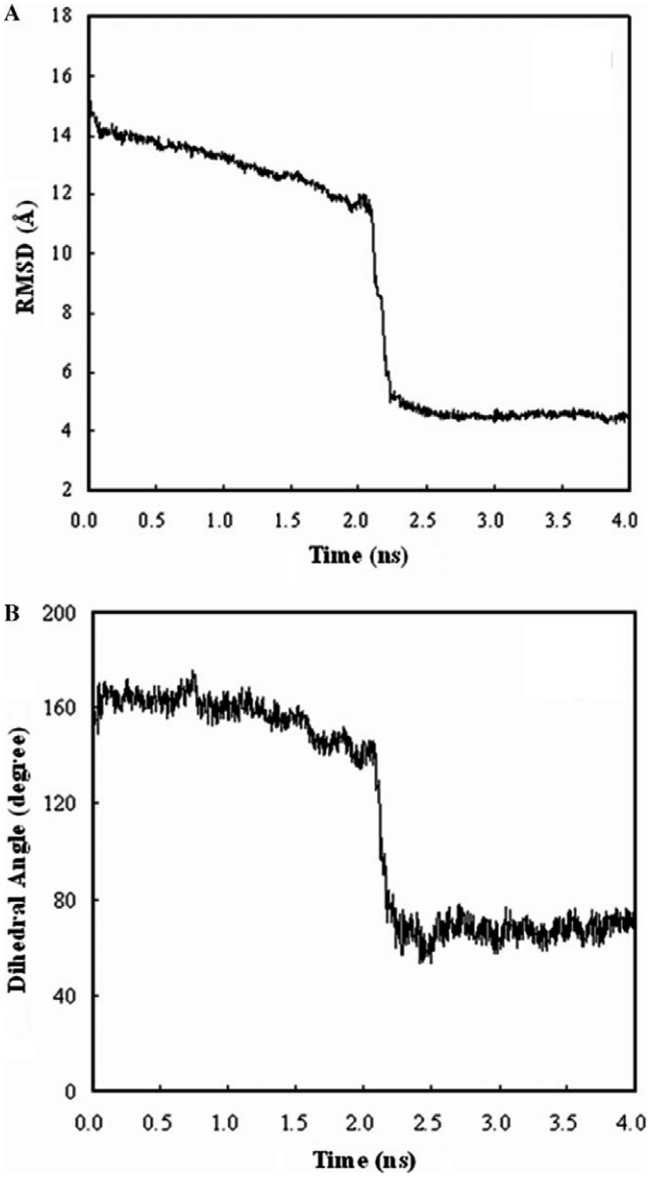

Fig. 2. Large conformational changes in G4–G6 during the activation-to-inactivation TMD simulation. Changes in (A) RMSD and (B) rotational angle of G6 as a function of simulation time.

the inactive G4–G6 was 15.08 Å. The RMSD gradually decreases to ~11.8 Å until ~2 ns and then sharply drops to ~5.0 Å. After this rapid drop takes place, the RMSD continues to decrease very gradually. The dihedral angle profile of Fig. 2B shows that G6 rapidly rotates ~90° at ~2 ns. The large conformational changes observed at ~2 ns are not artifacts due to the two-step weighting methods used in the activation-to-inactivation TMD simulation, because the 4 ns TMD simulation was performed in a continuous fashion without discrete changes in the constraint force constant.

Fig. 3 shows changes in interdomain distances as a function of the simulation time. In the period from the start of the simulation to ~2 ns, domains G4 and G6 rapidly approach each other, while domains G5 and G6 prepare to fall apart. At the period of the conformational rotation

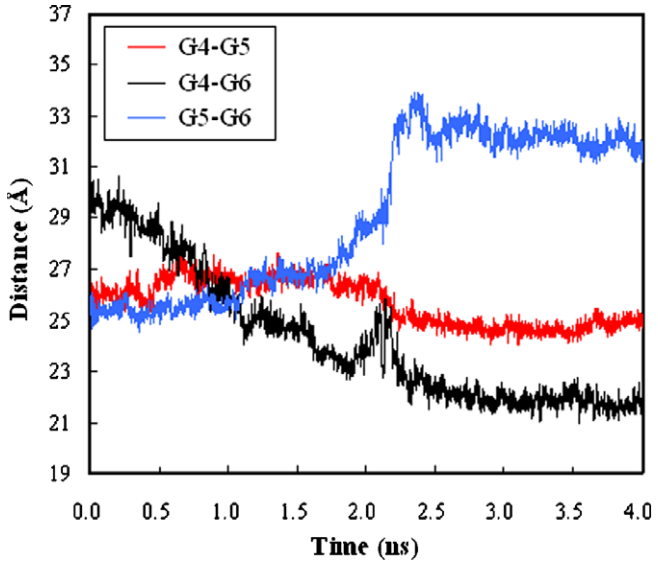

Fig. 3. Changes of interdomain distances in G4–G6 during the activation-to-inactivation TMD simulation.

of G6, the interdomain distance between G5 and G6 greatly increases and that between G4 and G5 slightly decreases. A strong peak is observed in the plot of the interdomain distance between G4 and G6 due to the rotation of G6. From the completion of the G6 domain rotation to the end of the simulation, there is little change in the interdomain distances because most large conformational changes were completed before this period.

We performed inactivation-to-activation TMD simulation as well as activation-to-inactivation TMD simulation. In vitro, activation involves the continuous β-sheet between domains G4 and G6 to be destabilized and then parted due to the binding of Ca^{2+} ions. The inactivation-to-activation TMD simulation system does not contain Ca^{2+} ions; instead, the β-sheet is severed by the applied artificial perturbation forces. We observed in the plot of the rotational angles that G6 in the inactivation-to-activation TMD simulation rotates in the opposite direction to that in the activation-to-inactivation TMD simulation (data not shown). This means that the large rotation of the G6 domain observed through the activation-to-inactivation and the inactivation-to-activation TMD simulations occurs through a single conformational pathway.

Contribution of calcium ions to gelsolin G4–G6 activation

To compare the relative affinities of calcium ions for their binding sites and to assess their contributions to the G4–G6 conformational changes, we measured the deviations from the original distance between the calcium ion and the CM of its binding site during the activation-to-inactivation TMD simulation (Fig. 4). The CM of the binding pocket was determined from the coordinates of the atoms that bind to the calcium ion. Ab initio simulation of Ca^{2+} binding and the transition pathway of gelsolin G4–G6 is computationally very difficult because commonly

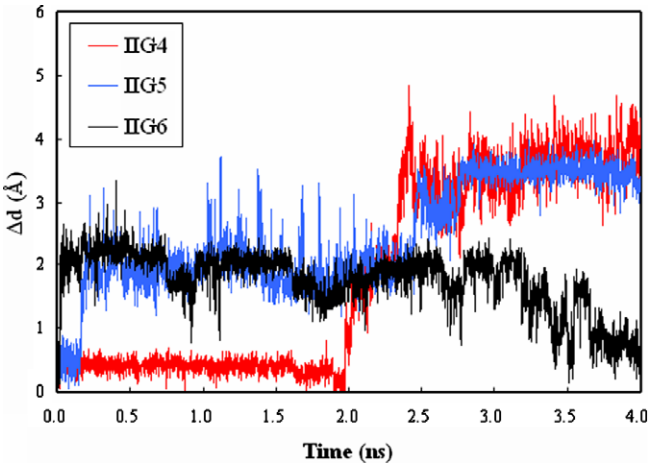

Fig. 4. Deviations of calcium ions from their binding sites during the activation-to-inactivation TMD simulation.

used simulations can only access processes occurring of the order of nanoseconds due to computation time constraints. An alternative approach to overcome this problem is to simulate the Ca^{2+} unbinding processes. Ca^{2+}-binding features obtained from the activation-to-inactivation TMD simulation may provide insight into the possible mechanisms of Ca^{2+} recognition during the activation of G4–G6.

The G4-bound Ca^{2+} (IIG4) maintains a stable binding state at its binding site until ~2 ns. After this point, IIG4 begins to deviate from its binding site, and the magnitude of the deviation rapidly increases until ~2.5 ns. To elucidate the relationship between these deviations of the Ca^{2+}-binding position and the local conformational changes at this site, we analyzed the change in distance between Ca^{2+}-binding residues during the activation-to-inactivation TMD simulation (Fig. 5). In the crystal structure of the inactive G4–G6, the distances between the CA atoms of Gly444-Thr524 (444–524) and Glu475-Thr524 (475–524) are 4.559 and 11.773 Å, respectively. In the crystal structure of the active G4–G6, on the other hand, these distances are 7.077 and 9.894 Å, respectively. Hence, local

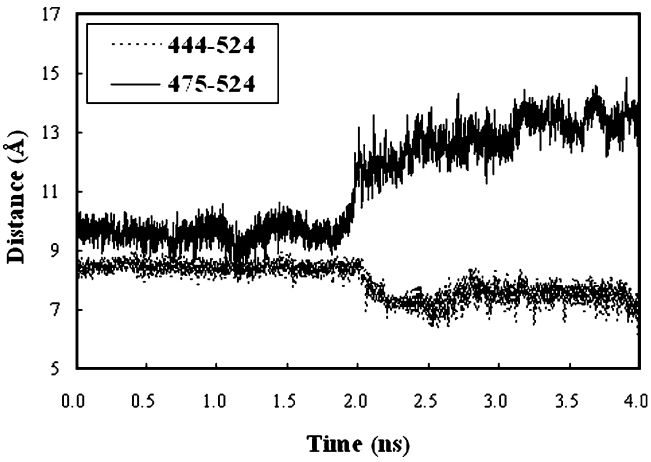

Fig. 5. Structural changes at the G4 Ca^{2+}-binding site. The plot shows time dependence of the distance between the CA atoms of Gly444 and Thr524 and of Glu475 and Thr524.

conformational changes take place at the IIG4-binding site along the G4–G6 activation pathway. Our simulation indicates that these local conformational changes begin to be observed at ~2 ns and result in the destabilization of the calcium ion bound to G4.

For Ca^{2+} bound to G5 (IIG5), increases in the deviations of distance were observed at two different points, ~0.16 ns and ~2.5 ns in Fig. 4. As in the case of IIG4, we measured the changes in distances between the CA atoms of Asp565 and Glu587 (565–587), and between the CG atom of Asp565 and the CZ atom of Arg629 (565–629) during the activation-to-inactivation TMD (Fig. 6A). In the crystal structure of the inactive G4–G6, Asp565 and Arg629 form a salt bridge, and the distances of 565–587 (CA–CA) and 565–629 (CG–CZ) are 6.092 and 4.543 Å, respectively. In the crystal structure of the active G4–G6, the distance of 565–587 (CA–CA) is 6.691 Å and that of 565–629 (CG–CZ) is 12.351 Å. Fig. 6A indicates that the decrease in Ca^{2+}-stability at ~2.5 ns is due to the change in the local conformation at the IIG5-binding site. To elucidate the cause of the instability of IIG5 at ~0.16 ns, we calculated the number of contacting residues between domains G5 and G6 during the TMD simulation (Fig. 6B). The residues between Gly620 and Met634 are located in the loop connecting domains G5 and G6. The G5–G6 loop deeply buried with a maximum number of contacts is destabilized with the decrease of an interface resulting from a tighter association within G5 and G6 at ~0.16 ns, which affects the stability of Ca^{2+} binding to G5.

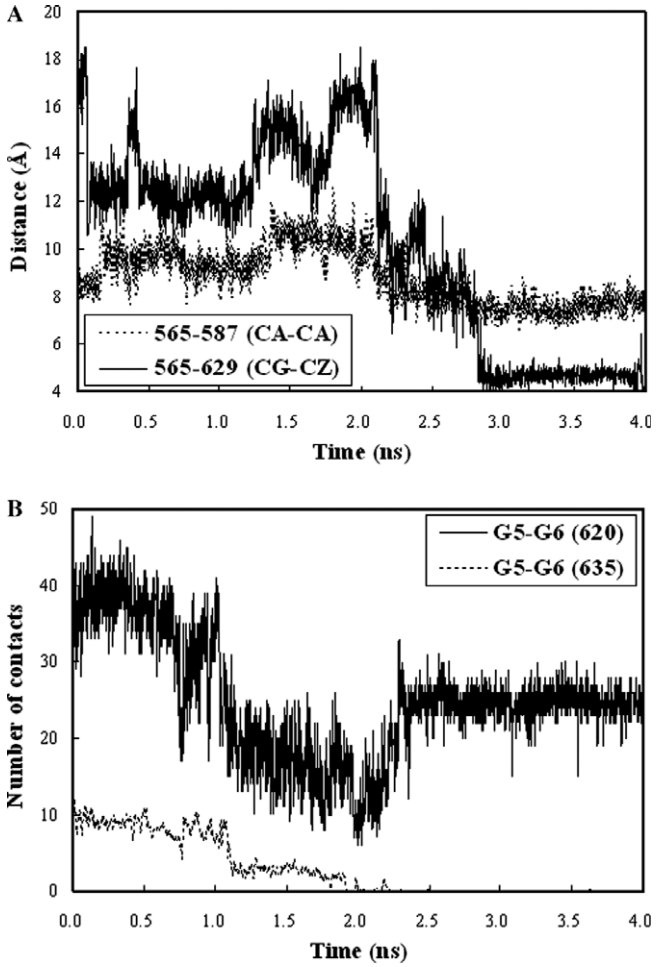

Fig. 6. Structural changes at the G5 Ca^{2+}-binding site. (A) Time dependence of the distance between the CA atoms of Asp565 and Glu587, and between the CG atom of Asp565 and the CZ atom of Arg629. (B) Number of contacts between G5 and G6. When the distance between the a CA atoms in G5 and G6 was within 7 Å, the pair was considered to be in contact. Here, two types of contact modes were considered. G5–G6 (620) is the number of contacts measured between G5 and residues 620–741 of G6. G5–G6 (635) is the number of contacts measured between G5 and residues 635–741 of G6.

The calcium ion bound to G6 (IIG6) is somewhat destabilized from the beginning of the simulation in Fig. 4, but the distance deviations gradually decrease after ~3 ns. At the end of the simulation, the distance deviation of IIG6 was the smallest among the three calcium ions. This result suggests that the binding affinity of Ca^{2+} may be the strongest for domain G6 because, in the inactive state, this site is closest to a Ca^{2+}-coordinating geometry.

Energetics of gelsolin G4–G6 activation

In the activation of gelsolin G4–G6, the standard free energy change is the difference between the free energies for the active and inactive G4–G6. The free energy change may be simply broken down to its main contributions as follows:

$$\Delta G = \Delta W - T\Delta S^{\text{confG4}} - T\Delta S^{\text{confG5}} - T\Delta S^{\text{confG6}} - T\Delta S^{\text{confLoop}}, \quad (2)$$

where W is the 'effective energy' or 'potential of mean force', which refers to the free energy of the system (protein plus solvent) for a fixed conformation of the molecule; that is, it consists of the intramolecular energy of the protein plus the solvation free energy [23].

$$W = H_{\text{intra}} + \Delta G^{\text{slv}} \quad (3)$$

$T\Delta S^{\text{confG4}}$, $T\Delta S^{\text{confG5}}$, and $T\Delta S^{\text{confG6}}$ are the entropy changes attributed to the local conformational changes at the G4, G5, and G6 binding sites upon Ca^{2+} binding, respectively, and $T\Delta S^{\text{confLoop}}$ is the entropy change attributed to the conformation changes in the G5–G6 loop during the activation of G4–G6.

We determined the averaged effective energy values from 500 ps equilibrium MD simulations for the inactive and the active G4–G6. The average energy over the final 300 ps for the inactive G4–G6 was −8103 kcal/mol. For the active G4–G6, the calculated effective energy values including or excluding nonbonded interaction energies between calcium ions and G4–G6 were −8226 kcal/mol and −7905 kcal/mol, respectively. These results indicate that the effective energy of inactive G4–G6 is lower than that of active G4–G6 but that the inactive G4–G6 is energetically stabilized by Ca^{2+} binding.

For Ca^{2+}-binding proteins, Kuroki et al. [24] evaluated the contribution of conformational changes at each binding site upon Ca^{2+} binding. They reported that, for the contribution of Ca^{2+} binding alone, the enthalpy increase is ~2 kcal/mol and the entropy release is ~10 kcal/mol. They also showed that after removing these thermodynamic contributions, the enthalpy change upon the binding of Ca^{2+} is negative but is almost compensated by the negative entropy change.

The rupture of the continuous β-sheet between G4 and G6 upon Ca^{2+} binding increases the enthalpy of G4–G6. This thermodynamically unfavorable contribution might be compensated by the entropy release of the G5–G6 loop. The distribution of the end-to-end distance, $P(r)$, and the entropy of a polypeptide chain, S, are given as follows [25]:

$$P(r) = 4\pi r^2 \left(\frac{3}{2\pi\langle r^2\rangle_0}\right)^{3/2} \exp(-3r^2/2\langle r^2\rangle_0)\mathrm{d}r \quad (4)$$

and

$$S = k_B \ln P(r), \quad (5)$$

where $\langle r^2\rangle_0$ is the average end-to-end distance of the random chain and k_B is Boltzmann's constant. After simplification, the difference in entropy between the unstressed state S and the stressed state S_0 can be expressed as

$$\Delta S = S - S_0 = -k\left(\frac{3(r^2 - r_0^2)}{2\langle r^2\rangle_0}\right) \quad (6)$$

The loop connecting G5 and G6 in the inactive G4–G6 has an extended chain conformation, whereas that in the active G4–G6 is somewhat folded. Therefore, the entropically unfavorable conformation of the loop in the active G4–G6 is willing to return to its stable conformation and facilitates the movement of G6. On the other hand, the association of G6 and G5 might again offset the entropic gain of the G5–G6 loop in inactive gelsolin G4–G6, similar to the characters in protein folding.

Discussion and conclusions

An important issue in the study of gelsolin is determining which of the currently identified Ca^{2+}-binding sites are physiologically relevant and how their occupancy affects conformational changes in gelsolin. To date, a number of studies have addressed these questions using biophysical and biochemical approaches, but none of these methods has provided a detailed molecular model of the large-scale conformational changes in the Ca^{2+}-sensitive half of gelsolin that occur following the addition of Ca^{2+} [5]. In the current study, we explored the conformational changes in G4–G6 using TMD simulations.

The assignment of the calcium-binding sites has been controversial. The 3.4 Å structure of G4–G6 in complex with actin showed that one type I Ca^{2+} and one type II Ca^{2+} bind to G4 [10]. Type II ions cause the conformational changes in gelsolin, whereas type I calcium ions regulate the interaction with actin. Based on a 3.0 Å structure of the C-terminal half of gelsolin in complex with actin, Choe et al. [14] found two additional type II calcium ions bound at G5 and G6. In contrast, a structure of active G4–G6 in the absence of actin suggested that the two Ca^{2+}-binding sites with the high affinities are in G5 and G6 [15]. A 2.0 Å structure of Ca^{2+}-activated G4–G6, however, indicated three bound type II Ca^{2+} ions, one each in G4, G5, and G6 [16]. The simulation results presented here indicate that the type II Ca^{2+} ions located in G4, G5, and G6 each have individual distinct biological roles in driving the conformational changes in the inactive form and stabilizing the activated form.

A number of studies have characterized the Ca^{2+}-binding affinities of gelsolin fragments. Isolated G4–G5 and G5–G6 each bind to a single calcium ion, with binding affinities of ~2 and ~0.2 μM, respectively [26], whereas the isolated single domains G4 or G5 did not bind Ca^{2+}. Although nanomolar concentrations of Ca^{2+} initiate the unlatching of the tail–G2 interaction that prevents whole gelsolin from binding, actin binding only occurs after Ca^{2+} reaches micromolar levels [27]. Protease susceptibility studies have shown that the loop between G5 and G6 is protected above 50 μM Ca^{2+}. These data indicate that a low-affinity calcium-binding site lies in G5 and that more than 100 μM Ca^{2+} is required to facilitate small conformational changes in the G5–G6 loop and finally stabilize actin binding [28].

Our MD simulations support the idea that Ca^{2+} ions bind to the domains in the order of G6, G4, and G5, with binding affinities of ~0.2, ~2, and ~100 μM, respectively. Alterations in the binding affinities of the calcium ions in these three domains appear to be related to local conformational changes at their binding sites. In the inactive, unlatched G4–G6 structure, the G6 site is close to a Ca^{2+}-binding geometry, while the conformations at the G4 and G5 binding sites are unsuitable for Ca^{2+} binding. Higher concentrations of Ca^{2+} coupled with the conformational changes induced through Ca^{2+} binding to G6 are required for occupation of these sites. The competence of gelsolin G4–G6 as a Ca^{2+} sensor can be attributed to small Ca^{2+}-induced conformational changes at each binding site. These local perturbations are converted into larger domain movements.

Based on the binding stability of calcium ions and the conformational changes of G4–G6 as determined by activation-to-inactivation TMD simulation along with the previously reported X-ray crystal structure [10,14–16], we propose a three-phase scheme to describe the activation pathway of G4–G6 (Fig. 7).

Phase I—In inactive G4–G6, the β-sheet of G4 is linked continuously to that of G6, and the long helix of G6 is kinked to keep it from clashing with the helix of G4. Ca^{2+}-ligating residues Asp669 and Asp670 interact with Arg168 and Arg169 from G1–G3. Upon increase of the Ca^{2+} concentration, the G6 Ca^{2+}-binding site initially becomes occupied. The energetic preference for Ca^{2+}

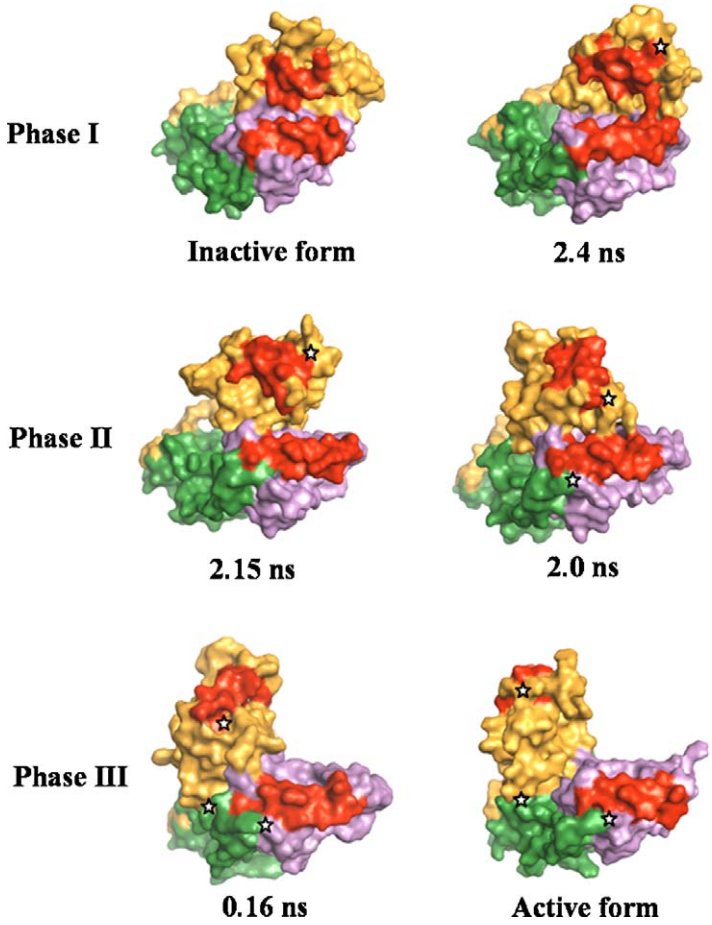

Fig. 7. Surface representation of the structure of gelsolin domains G4–G6 during the activation-to-inactivation TMD. Snapshots of biased potential-induced conformational changes are shown in reverse order. The long helixes in G4 and G6 are shown in red. Type II calcium ions are also represented with star-shaped symbols. The conformational change pathway is divided into three phases based on our interpretation of the TMD simulations. (For interpretation of the references to color in this figure legend, the reader is referred to the web version of this paper.)

binding, the breakage of the ionic interactions between Ca^{2+}-ligating residues and G1–G3, and G6 helix straightening result in the destabilization of the continuous β-sheet between G4 and G6.

Phase II—Detachment of G6 from G4 and a rotation of G6 coincide with the occupation of the G4 Ca^{2+}-binding site. During this process, local conformational changes begin to occur at the G4 and the G5 Ca^{2+}-binding sites. The IIG4 Ca^{2+} ion contributes to local conformational changes at the binding site in G4 and alters the relative positioning between domains G4 and G5. This repositioning pulls on the G5–G6 linker, further destabilizing the latched structure between G4 and G6, and accelerating the disengagement of these two domains. This repositioning has a knock-on effect in translating the G5–G6 linker, preventing G6 from binding to G4 and accelerating the disengagement of these two domains. Once G4 and G6 are fully detached, the major conformational changes in G4–G6 occur, including a large rotation of G6.

Phase III—G6 and a calcium ion synergistically dock to G5 to recover the entropic loss of the G5–G6 loop in inactive gelsolin G4–G6 and to increase the number of contacts between G5 and G6. After the occupation of the G4 Ca^{2+}-binding site, the G5 Ca^{2+} ion facilitates the creation of the new G5–G6 interface through local conformational changes, which finally stabilizes the structure of activated G4–G6.

Taken together, the present work implies an interesting mechanism of the conformational change of the gelsolin C-terminal half based on the first all-atom computer simulation of the molecule. It also suggests binding stabilities of Ca^{2+} ions at their binding sites and their binding orders which cannot be directly obtained by current biophysical and biochemical experiments.

Acknowledgments

This study was supported by the International Mobile Telecommunications 2000 R&D Project (01-PJ11-PG9-01BT00B-0019) from the Ministry of Information & Communication, Republic of Korea and a Korea Research Foundation Grant.

References

[1] T.D. Pollard, L. Blanchoin, R.D. Mullins, Molecular mechanisms controlling actin filament dynamics in nonmuscle cells, Annu. Rev. Biophys. Biomol. Struct. 29 (2000) 545–576.

[2] H.Q. Sun, M. Yamamoto, M. Mejillano, H.L. Yin, Gelsolin, a multifunctional actin regulatory protein, J. Biol. Chem. 274 (1999) 33179–33182.

[3] J.H. Hartwig, Mechanisms of actin rearrangements mediating platelet activation, J. Cell Biol. 118 (1992) 1421–1442.

[4] P.G. Allen, Actin filament uncapping localizes to ruffling lamellae and rocketing vesicles, Nat. Cell Biol. 5 (2003) 972–979.

[5] A.M. McGough, C.J. Staiger, J.K. Min, K.D. Simonetti, The gelsolin family of actin regulatory proteins: modular structures, versatile functions, FEBS Lett. 552 (2003) 75–81.

[6] F. Ressad, D. Didry, G.X. Xia, Y. Hong, N.H. Chua, D. Pantaloni, M.F. Carlier, Kinetic analysis of the interaction of actin-depolymerizing factor (ADF)/cofilin with G- and F-actins. Comparison of plant and human ADFs and effect of phosphorylation, J. Biol. Chem. 273 (1998) 20894–20902.

[7] L.D. Burtnick, E.K. Koepf, J. Grimes, E.Y. Jones, D.I. Stuart, P.J. McLaughlin, R.C. Robinson, The crystal structure of plasma gelsolin: implications for actin severing, capping, and nucleation, Cell 90 (1997) 661–670.

[8] D.J. Kwiatkowski, T.P. Stossel, S.H. Orkin, J.E. Mole, H.R. Colten, H.L. Yin, Plasma and cytoplasmic gelsolins are encoded by a single gene and contain a duplicated actin-binding domain, Nature 323 (1986) 455–458.

[9] P.J. McLaughlin, J.T. Gooch, H.G. Mannherz, A.G. Weeds, Structure of gelsolin segment 1-actin complex and the mechanism of filament severing, Nature 364 (1993) 685–692.

[10] R.C. Robinson, M. Mejillano, V.P. Le, L.D. Burtnick, H.L. Yin, S. Choe, Domain movement in gelsolin: a calcium-activated switch, Science 286 (1999) 1939–1942.

[11] L.D. Burtnick, D. Urosev, E. Irobi, K. Narayan, R.C. Robinson, Structure of the N-terminal half of gelsolin bound to actin: roles in severing, apoptosis and FAF, EMBO J. 23 (2004) 2713–2722.

[12] J. Bryan, Gelsolin has three actin-binding sites, J. Cell Biol. 106 (1988) 1553–1562.

[13] T. Hellweg, H. Hinssen, W. Eimer, The Ca(2+)-induced conformational change of gelsolin is located in the carboxyl-terminal half of the molecule, Biophys. J. 65 (1993) 799–805.

[14] H. Choe, L.D. Burtnick, M. Mejillano, H.L. Yin, R.C. Robinson, S. Choe, The calcium activation of gelsolin: insights from the 3A structure of the G4-G6/actin complex, J. Mol. Biol. 324 (2002) 691–702.

[15] S. Kolappan, J.T. Gooch, A.G. Weeds, P.J. McLaughlin, Gelsolin domains 4–6 in active, actin-free conformation identifies sites of regulatory calcium ions, J. Mol. Biol. 329 (2003) 85–92.

[16] K. Narayan, S. Chumnarnsilpa, H. Choe, E. Irobi, D. Urosev, U. Lindberg, C.E. Schutt, L.D. Burtnick, R.C. Robinson, Activation in isolation: exposure of the actin-binding site in the C-terminal half of gelsolin does not require actin, FEBS Lett. 552 (2003) 82–85.

[17] A. Fiser, A. Sali, ModLoop: automated modeling of loops in protein structures, Bioinformatics 19 (2003) 2500–2501.

[18] T. Lazaridis, M. Karplus, Effective energy function for proteins in solution, Proteins 35 (1999) 133–152.

[19] Y. Marcus, Thermodynamics of solvation of ions: part 5. Gibbs free energy of hydration at 298.15 K, J. Chem. Soc. Faraday Trans. 87 (1991) 2995.

[20] J. Schlitter, M. Engels, P. Krüger, E. Jacoby, A. Wollmer, Targeted molecular dynamics simulation of conformational change: application to the T-R transition in insulin, Mol. Simul. 10 (1993) 291–309.

[21] C.L. Brooks, M. Karplus, Deformable stochastic boundaries in molecular dynamics, J. Chem. Phys. 79 (1983) 6312–6325.

[22] S. Nose, A molecular dynamics method for simulations in the canonical ensemble, Mol. Phys. 52 (1984) 255–268.

[23] T. Lazaridis, G. Archontis, M. Karplus, Enthalpic contribution to protein stability: insights from atom-based calculations and statistical mechanics, Adv. Protein Chem. 47 (1995) 231–306.

[24] R. Kuroki, K. Nitta, K. Yutani, Thermodynamic changes in the binding of Ca^{2+} to a mutant human lysozyme (D86/92), J. Biol. Chem. 267 (1992) 24297–24301.

[25] U.F. Gedde, Polymer Physics, Chapman & Hall, London, UK, 1995.

[26] B. Pope, S. Maciver, A. Weeds, Localization of the calcium-sensitive actin monomer binding site in gelsolin to segment 4 and identification of calcium binding sites, Biochemistry 34 (1995) 1583–1588.

[27] B.J. Pope, J.T. Gooch, A.G. Weeds, Probing the effects of calcium on gelsolin, Biochemistry 36 (1997) 15848–15855.

[28] S. Khaitlina, M. Walloscheck, H. Hinssen, Calcium-induced conformational changes in the C-terminal half of gelsolin stabilize its interaction with the actin monomer, Biochemistry 43 (2004) 12838–12845.